



# 1 **Interpreting Space-Based Trends in Carbon Monoxide**

2

3 Sarah A. Strode<sup>1,2</sup>, Helen M. Worden<sup>3</sup>, Megan Damon<sup>2,4</sup>, Anne R. Douglass<sup>2</sup>, Bryan N.  
4 Duncan<sup>2</sup>, Louisa K. Emmons<sup>3</sup>, Jean-Francois Lamarque<sup>3</sup>, Michael Manyin<sup>2,4</sup>, Luke D.  
5 Oman<sup>2</sup>, Jose M. Rodriguez<sup>2</sup>, Susan E. Strahan<sup>1,2</sup>, Simone Tilmes<sup>3</sup>

6

7 <sup>1</sup>Universities Space Research Association, Columbia, MD, USA

8 <sup>2</sup>NASA Goddard Space Flight Center, Greenbelt, MD, USA

9 <sup>3</sup>National Center for Atmospheric Research, Boulder, CO, USA

10 <sup>4</sup>Science Systems and Applications, Inc., Lanham, MD, USA

11

12 *Correspondence to:* S. A. Strode (sarah.a.strode@nasa.gov)

## 13 **Abstract**

14 We use a series of chemical transport model and chemistry climate model simulations to  
15 investigate the observed negative trends in MOPITT CO over several regions of the  
16 world, and to examine the consistency of time-dependent emission inventories with  
17 observations. We find that simulations driven by the MACCity inventory, used for the  
18 Chemistry Climate Modeling Initiative (CCMI), reproduce the negative trends in the CO  
19 column observed by MOPITT for 2000-2010 over the eastern United States and Europe.  
20 However, the simulations have positive trends over eastern China, in contrast to the  
21 negative trends observed by MOPITT. The model bias in CO, after applying MOPITT  
22 averaging kernels, contributes to the model-observation discrepancy in the trend over  
23 eastern China. The total ozone column plays a role in determining the simulated  
24 tropospheric CO trends. A large positive anomaly in the simulated total ozone column in  
25 2010 leads to a negative anomaly in OH and hence a positive anomaly in CO,  
26 contributing to the positive trend in simulated CO.

## 27 **1. Introduction**

28

29 Carbon monoxide (CO) is an air pollutant that contributes to ozone formation and  
30 affects the oxidizing capacity of the troposphere (Thompson, 1992; Crutzen, 1973). Its  
31 primary loss is through reaction with OH, which leads to a lifetime of 1-2 months (Bey et  
32 al., 2001) and makes CO an excellent tracer of long-range transport. Both fossil fuel



33 combustion and biomass burning are major sources of CO. The biomass burning source  
34 shows large interannual variability (van der Werf et al., 2010), while fossil fuel emissions  
35 typically change more gradually. The time-dependent MACCity inventory (Granier et  
36 al., 2011) shows decreases in CO emissions from the United States and Europe from  
37 2000 to 2010 due to increasing pollution controls, but increases in emissions from China.  
38 MACCity emissions for years after 2000 are based on the Representative Concentration  
39 Pathway (RCP) 8.5 (Riahi et al., 2007). The REAS (Kurokawa et al., 2013) and  
40 EDGAR4.2 (EC-JRC/PBL, 2011) inventories also show increasing CO emissions from  
41 China. The bottom-up inventory of Zhang et al. (2009) shows an 18% increase in CO  
42 emissions from China from 2001 to 2006, and Zhao et al. (2012) estimate a 6% increase  
43 between 2005 and 2009. However, there is considerable uncertainty in bottom-up  
44 inventories, and comparison of model hindcast simulations driven by bottom-up  
45 inventories with observations provides an important test of the time-dependent emission  
46 estimates.

47 Space-based observations of CO are now available for over a decade and show  
48 trends at both hemispheric and regional scales. Warner et al. (2013) found significant  
49 trends in both background CO and recently emitted CO at 500 hPa over southern  
50 hemisphere oceans and northern hemisphere land and ocean in Atmospheric Infrared  
51 Sounder (AIRS) data. Worden et al. (2013) calculated trends in the CO column from  
52 several thermal infrared (TIR) instruments including MOPITT and AIRS. They found  
53 statistically significant negative trends over Europe, the eastern United States, and China  
54 for 2002-2012. He et al. (2013) also report a negative trend in MOPITT near-surface CO  
55 over western Maryland.

56 Surface concentrations of CO show downward trends over the United States  
57 driven by emission reductions (EPA, 2011), consistent with the space-based trends.  
58 Decreases in the partial column of CO from FTIR stations in Europe also show decreases  
59 from 1996 to 2006, consistent with emissions decreases (Angelbratt et al., 2011). Yoon  
60 and Pozzer (2014) found that a model simulation of 2001 to 2010 reproduced negative  
61 trends in surface CO over the eastern U.S. and western Europe, but showed a positive  
62 trend in surface CO over southern Asia.



63           The cause of the negative trend over China seen in MOPITT and AIRS data is  
64 uncertain. The trend is consistent with the results of (Li and Liu, 2011), who found  
65 decreases in surface CO measurements in Beijing, and with decreases in CO emissions in  
66 2008 inferred from the correlation of CO with CO<sub>2</sub> measured at Hateruma Island  
67 (Tohjima et al., 2014) and at a rural site in China (Wang et al., 2010). Yumimoto et al.  
68 (2014) used inverse modeling of MOPITT data to infer a decrease in CO emissions from  
69 China after 2007. The 2008 Olympic Games and the 2009 global economic slowdown  
70 led to reductions in CO (Li and Liu, 2011; Worden et al., 2012). However, the negative  
71 trend in MOPITT CO is inconsistent with the rising CO emissions of the MACCity and  
72 REAS inventories. Inverse modeling of MOPITT version 6 data yields a negative trend  
73 in CO emissions from China and a larger global decline in CO emissions than that found  
74 in the MACCity inventory (Yin et al., 2015).

75           This study examines whether global hindcast simulations can reproduce the trends  
76 and variability in carbon monoxide seen in the MOPITT record. We examine the role of  
77 averaging kernels and the contribution of trends at different altitudes to the trends  
78 observed by MOPITT. We then examine the impact of OH variability on the simulated  
79 trends in CO.

## 80 **2. Methods**

### 81 **2.1. MOPITT**

82           The MOPITT instrument onboard the Terra Satellite provides the longest satellite-  
83 based record of atmospheric CO, with observations available from March 2000 to  
84 present. It provides nearly global coverage every three days (Edwards et al., 2004). We  
85 use the Level 3 column data from the Version 5 TIR product, which has negligible drift  
86 in the bias over time (Deeter et al., 2013).

87           We calculate trends and de-seasonalized anomalies for the Eastern U.S., Europe, and  
88 eastern China regions described by Worden et al. (2013). Trends that differ from zero by  
89 more than the two-sigma uncertainty on the trend are considered statistically significant.  
90 We account for autocorrelation of the data when calculating the uncertainty on the trends.  
91 We calculate the annual cycle by fitting the data with a series of sines and cosines as well  
92 as the linear trend, and then remove the annual cycle to obtain the de-seasonalized



93 anomalies. Months with insufficient data are excluded from the trend analysis. We  
94 report the MOPITT trends for 2000-2010 and 2000-2011 for comparison with model  
95 simulations, and for 2000-2014 to give a longer-term view of the observed trends.

96

## 97 **2.2. Model Simulations**

98 We use a suite of chemistry climate model (CCM) and chemical transport model  
99 (CTM) simulations to interpret the observed trends. The Global Modeling Initiative  
100 (GMI) CTM includes both tropospheric (Duncan et al., 2007) and stratospheric (Strahan  
101 et al., 2007) chemistry, including over 400 reactions and 124 chemical species.  
102 Meteorology for the GMI simulations comes from the Modern-Era Retrospective  
103 Analysis for Research and Applications (MERRA) (Rienecker et al., 2011). The GEOS-  
104 5 Chemistry Climate Model (GEOSCCM)(Oman et al., 2011) incorporates the GMI  
105 chemical mechanism into the GEOS-5 atmospheric general circulation model (AGCM).  
106 The GEOSCCM simulations are forced by observed sea surface temperatures (SSTs)  
107 from (Reynolds et al., 2002).

108 The Community Earth System Model, CESM1 CAM4-chem, includes 191 chemical  
109 tracers and over 400 reactions for both troposphere and stratosphere (Tilmes et al., 2016).  
110 The model can be run fully coupled to a free-running ocean, with prescribed SSTs, or  
111 with nudged meteorology from GEOS-5 or MERRA analysis. CESM1 CAM4-chem is  
112 further coupled to the land model, providing biogenic emissions from the Model of  
113 Emissions and Aerosols from Nature (MEGAN), version 2.1 (Guenther et al., 2012).

114 Several simulations were conducted as part of the Chemistry-Climate Model Initiative  
115 (CCMI) project (Eyring et al., 2013). These include the Ref-C1 simulation of the  
116 GEOSCCM and a Ref-C1 CESM1 CAM4-Chem simulation, hereafter called G-Ref-C1  
117 and C-Ref-C1, respectively, and the Ref-C1-SD simulation of the GMI CTM. Both the  
118 Ref-C1 and the Ref-C1-SD simulations use time-dependent anthropogenic and biomass  
119 burning emissions from the MACCity inventory (Granier et al., 2011), but the Ref-C1-  
120 SD simulations use specified meteorology while the Ref-C1 simulations run with  
121 prescribed SSTs.

122 Given the uncertainty in CO emissions, we conduct a GMI CTM simulation using an  
123 alternative time-dependent emissions scenario, called AltEmis. This simulation is



124 described in detail in (Strode et al., 2015b). Briefly, anthropogenic emissions include  
125 time-dependence based on EPA (<http://www.epa.gov/ttn/chieftrends/index.html>), the  
126 REAS inventory (Ohara et al., 2007), and EMEP  
127 ([http://www.ceip.at/ms/ceip\\_home1/ceip\\_home/webdab\\_emepdatabase/reported\\_emissio](http://www.ceip.at/ms/ceip_home1/ceip_home/webdab_emepdatabase/reported_emissio)  
128 [ndata](http://www.ceip.at/ms/ceip_home1/ceip_home/webdab_emepdatabase/reported_emissio)), and annual scaling's from (van Donkelaar et al., 2008). Biomass burning  
129 emissions are based on the GFED3 inventory (van der Werf et al., 2010). While the  
130 regional emission trends in this simulation are of the same sign as in the Ref-C1 case, the  
131 magnitude of the negative trends over the U.S. and Europe are smaller and the positive  
132 trend over China is larger, leading to a positive global trend (Fig. 1). We also conduct a  
133 sensitivity study called EmFix with anthropogenic and biomass burning emissions held  
134 constant at year 2000 levels. Table 1 summarizes the simulations used in this study.

135 We convolve the simulated CO with the MOPITT averaging kernels and a priori in  
136 order to compare the simulated and observed CO columns. The averaging kernels are  
137 space and time dependent. We use the following equation from (Deeter et al., 2013):

$$138 \quad C_{\text{sim}} = C_0 + A(X_{\text{mod}} - X_0) \quad (1)$$

139 Where  $C_{\text{sim}}$  and  $C_0$  are the simulated and a priori CO total columns, respectively,  $A$  is the  
140 total column averaging kernel, and  $X_{\text{mod}}$  and  $X_0$  are the modeled and a priori CO profiles,  
141 respectively.

142 We deseasonalize the simulated CO columns and calculate their linear trend  
143 following the same procedure that we applied to the MOPITT CO. Months that do not  
144 have MOPITT data (June-July 2001 and August-September 2009) are excluded from the  
145 analysis of the model trends as well.

146 The Ref-C1 and Ref-C1-SD simulations requested by CCMI extend until 2010.  
147 However, the MACCity biomass burning emissions extend only until 2008. CAM4-  
148 Chem therefore repeated the biomass burning emissions for 2008 for years 2009-2010.  
149 In contrast, the GEOSCCM Ref-C1 and GMI Ref-C1-SD simulations used emissions  
150 from GFED3 (van der Werf et al., 2010) for years after 2008. We also report the  
151 simulated and MOPITT trends for both 2000-2010 and 2000-2011 since some  
152 simulations are only available to 2010, while others continued through 2011. Figure S1  
153 in the supplemental information shows results extended through 2011.



## 154 **3. Results**

### 155 **3.1. Trends over Europe, the United States, and the Northern Hemisphere**

156 The hindcast simulations driven by MACCity emissions (G-Ref-C1, Ref-C1-SD, and  
157 C-Ref-C1) show negative trends in CO over the U.S. and Europe that agree with the  
158 observed slope from MOPITT within the uncertainty (Fig. 2, Table 2). The MOPITT  
159 trends for both regions are statistically significant for both regions, as shown by Worden  
160 et al. (2013). These results are consistent with the findings of Yin et al. (2015), whose  
161 inversion of MOPITT data showed a posteriori trends in CO emissions over the U.S. and  
162 western Europe that were consistent with but slightly larger than the a priori trends. The  
163 EmFix hindcast shows a positive, though non-significant, trend for both regions,  
164 indicating that the decrease in CO emissions is necessary for reproducing the downward  
165 trend in the CO column. The AltEmis simulation fails to produce the negative trends,  
166 despite including negative trends in regional emissions for both the U.S. and Europe.  
167 The impact of these negative regional trends is insufficient to overcome the positive  
168 global emission trend in the AltEmis scenario (Fig. 1), leading to positive trends in CO.

169 Figure 2 also reveals a negative bias in the simulated CO column between the models  
170 and MOPITT. A low bias in simulated CO at northern latitudes is often present in global  
171 models (Naik et al., 2013), and may indicate a high bias in northern hemisphere OH  
172 (Strode et al., 2015a) or CO dry deposition (Stein et al., 2014), as well as an  
173 underestimate of CO emissions.

174 The deseasonalized anomalies in the MOPITT and simulated CO columns are shown  
175 in Fig. 2b,d, and the correlation coefficient between the observed and simulated monthly  
176 anomalies are presented in Table 2b. The highest correlations are for the AltEmis and  
177 Ref-C1-SD simulations of the GMI CTM. This result is consistent with the use of year-  
178 specific meteorology, which we expect to better match the transport of particular years.  
179 The lowest correlations are for the EmFix simulation. This is expected since the EmFix  
180 simulation does not include inter-annual variability (IAV) in biomass burning. The IAV  
181 in biomass burning makes a large contribution to the IAV of CO (Voulgarakis et al.,  
182 2015).



183 The role of biomass burning in driving the CO variability is even more evident at the  
184 hemispheric scale. Figure 2g,h shows the anomalies in MOPITT and the simulations for  
185 the northern hemisphere (0-60N). The EmFix simulation shows almost no correlation,  
186 while the other simulations have correlation coefficients exceeding 0.6 (Table 2). The  
187 role of changing anthropogenic emissions is also evident, as the Ref-C1-SD simulation  
188 captures the 2008-2009 dip in the CO column while the EmFix simulation does not.  
189 Gratz et al. (2015) found decreasing CO concentrations at Mount Bachelor Observatory  
190 in Oregon during spring for 2004-2013, which they attribute to reductions in emissions  
191 leading to a lower hemispheric background. We also note that Ref-C1-SD and G-Ref-  
192 C1 have similar correlations with the observed variability for the northern hemisphere  
193 (Table 2), indicating that transport differences are less important for variability at the  
194 hemispheric scale.

### 195 3.2. Trend over China

196 Observations from MOPITT show a negative trend in the CO column over eastern  
197 China for 2002-2012 (Worden et al., 2013). The negative trend for the years 2000-2014  
198 exceeds that for 2000-2011 (Table 2), showing that it is not driven solely by temporary  
199 emission reductions in 2008. Our simulations do not reproduce this trend, and instead  
200 show increases in the CO column (Fig. 2e, S1e), which is expected given that CO  
201 emissions from China increase in four of the five simulations. The anomalies (Fig. 2f,  
202 S1f) show that the discrepancy in the simulated versus observed trends is driven largely  
203 by the failure of the simulations to capture the 2008 dip in the CO column. This suggests  
204 emission reductions in China during this time period are not adequately captured by the  
205 emission inventories. However, the good agreement between the observed and simulated  
206 decreases in CO for the northern hemisphere as a whole (Fig. 2g,h) suggest that on a  
207 global scale, the emission time series is reasonable. Consequently, we examine several  
208 other factors that may contribute to the difference in sign between the MOPITT and  
209 simulated CO trends.

210 Regional trends in CO are expected to vary with altitude, with surface concentrations  
211 most heavily influenced by local emissions. MOPITT TIR retrievals have higher  
212 sensitivity to CO in the mid-troposphere than at the surface (Deeter et al., 2004), so the  
213 trend in the MOPITT CO column will be weighted towards the trends in free tropospheric



214 CO rather than near-surface CO. We quantify this impact on our Ref-C1-SD CO column  
215 trends by comparing the trend in the pure-model CO column with that of the simulated  
216 column convolved with the MOPITT averaging kernels.

217 The simulated CO trend over eastern China for 2000-2011 is positive (but not  
218 significant) both with and without the averaging kernels, but application of the MOPITT  
219 kernels increases the positive trend from  $1.0 \cdot 10^{16}$  molec cm<sup>-2</sup> yr<sup>-1</sup> to  $1.3 \cdot 10^{16}$  molec cm<sup>-2</sup>  
220 yr<sup>-1</sup>. This result is initially surprising since we expect trends in the mid-troposphere to be  
221 more strongly influenced by the decrease in the hemispheric CO background. Indeed, the  
222 trends in CO concentration over eastern China simulated in Ref-C1-SD switch from  
223 positive in the lower troposphere to negative in the middle and upper troposphere.  
224 However, the application of the kernels results in more positive (or less negative) trends  
225 in all regions.

226 Yoon et al. (2013) show that since the averaging kernels vary over time, a bias  
227 between the true atmosphere and the a priori assumed by MOPITT can lead to an  
228 artificial trend in the retrieved CO. Similarly, the bias between the simulated CO  
229 concentrations and the MOPITT a priori, evident in Figure 2, can lead to an artifact in the  
230 simulated CO trend when the simulation is convolved with the MOPITT averaging  
231 kernels and a priori via equation 1. This is due to the changing contribution of the a  
232 priori when the vertical sensitivity (averaging kernel) is varying in time. MOPITT  
233 vertical sensitivity varies with time due to instrument degradation as well as the change in  
234 CO abundance.

235 We quantify this effect by convolving the simulated CO for each year with the  
236 MOPITT averaging kernels for the year 2008, thus removing the effect of the time-  
237 dependence of the averaging kernels. The resulting trend,  $0.42 \cdot 10^{16}$  molec cm<sup>-2</sup> yr<sup>-1</sup>, is  
238 less positive than the pure model trend or the original simulated trend. Thus, accounting  
239 for the time-dependence of the averaging kernels convolved with model bias reduces but  
240 does not eliminate the discrepancy with the observed trend. Other regions also show a  
241 more negative trend when the same averaging kernel is applied to the model results for  
242 all years. The large bias in CO at middle and high northern latitudes commonly seen in  
243 modeling studies thus impacts the ability of models to reproduce and attribute observed  
244 trends in satellite data.





245 Figure 2 and Table 2 also show a positive trend in the GMI EmFix simulation for  
246 eastern China. This larger trend in the EmFix simulation than the Ref-C1-SD simulation  
247 indicates that the net decrease in emissions contributes to decreasing CO over eastern  
248 China, consistent with the observed negative trend, but other factors in the model cause  
249 an increase in CO over eastern China even when all emissions are constant. The trend in  
250 the EmFix simulation thus contributes to the erroneous sign of the trend in the GMI  
251 simulations. The trends in the EmFix simulation for the northern hemisphere average and  
252 the eastern U.S. and Europe are positive as well (Table 2). We examine their cause in the  
253 next section.

### 254 3.3. Contribution of OH Interannual Variability

255

256 Since the EmFix simulation shows a positive trend in the northern hemisphere, we  
257 next examine the variability in the CO sink, OH. We also examine variability in the total  
258 ozone column, since overhead ozone is a major driver of OH variability (Duncan and  
259 Logan, 2008). Figure 3 shows the variability in CO and OH in the EmFix simulation.  
260 The positive and negative anomalies in CO correspond with the negative and positive  
261 anomalies, respectively, in OH. The anomalies in OH are in turn inversely related to  
262 anomalies in the total ozone column. The large NH ozone anomaly in 2010, in particular,  
263 leads to a large anomaly in OH and thus CO. The large CO anomaly near the end of the  
264 time series contributes to the apparent 11-year trend.

265 The large anomaly in the simulated total ozone column in 2010 is overestimated  
266 compared to observations. Figure 4 shows the time-dependence of the total ozone  
267 column from 30°-60°N in EmFix compared to SBUV data (Frith et al., 2014). While the  
268 observations show an anomaly in 2010, the magnitude is smaller than that produced by  
269 the simulation.

270 While the impact of OH interannual variability on the apparent trend in CO is clear in  
271 the EmFix simulation, this source of variability can be masked by large interannual  
272 variability in CO emissions in the other simulations. We examine the correlation  
273 between the de-trended and deseasonalized CO anomalies from 10°S-10°N in the Ref-  
274 C1-SD simulation and the CO emissions as well as the simulated OH and column ozone.  
275 Since the CO emitted in a given month can influence concentrations for several



276 subsequent months, we use a 3-month smoothing of the emission time series. We find a  
277 high correlation ( $r^2=0.78$ ) between the CO anomalies and the CO emissions. This  
278 correlation is also evident in the MOPITT data, as the MOPITT CO anomalies have a  
279 correlation of  $r^2=0.49$  with the emissions. Figure 5 shows the strong relationship between  
280 the simulated CO anomalies and the CO emissions. However, the colors in Fig. 5  
281 indicate that the scatter for a given level of emissions is often linked to the OH  
282 anomalies, with low/high OH anomalies leading to CO that is higher/lower than would be  
283 predicted just from the CO emissions. We find that the  $10^{\circ}\text{S}$ - $10^{\circ}\text{N}$  OH in the Ref-C1-SD  
284 simulation is anticorrelated with CO ( $r^2=0.33$ ) and with the total ozone column ( $r^2=0.45$ ).  
285 Consequently, the simulated ozone column plays a role in modulating tropical CO  
286 variability even when variable CO emissions are included, although the emissions still  
287 play the strongest role.

#### 288 4. Conclusions

289 We conducted a series of multi-year simulations to analyze the causes of the negative  
290 trends in MOPITT CO reported by (Worden et al., 2013). Both CTM and CCM  
291 simulations driven by the MACCity emissions reproduce the observed trends over the  
292 eastern U.S. and Europe, providing confidence in the regional emission trends.

293 None of the simulations reproduce the observed negative trend over eastern China.  
294 This negative trend persists even with the MOPITT data extended out to 2014. The  
295 MOPITT averaging kernels are weighted towards the free troposphere, where the relative  
296 importance of hemispheric versus local trends is greater. However, our simulations  
297 indicate that this effect is insufficient to explain the negative trends over China. While  
298 this likely indicates a too positive emission trend for China, several other factors play a  
299 role in the model-observation mismatch. We find that the time-dependent MOPITT  
300 averaging kernels, combined with the low bias in simulated CO, provides a positive  
301 component to the simulated trends. Large anomalies in the simulated ozone column in  
302 the GMI CTM simulations also contribute a positive component to the northern  
303 hemisphere trends due to their impact on OH.

304 Variability in emissions is the primary driver of year-to-year variability in simulated  
305 CO, but OH variability also plays a role. The simulated OH is anti-correlated with both



306 CO and the total ozone column, highlighting the importance of realistic overhead ozone  
307 columns for accurately simulating CO variability and trends. In addition, further work is  
308 needed to understand recent changes in CO emissions from China.

309

### 310 **Acknowledgements**

311 This work was supported by NASA's Modeling, Analysis, and Prediction program  
312 and computing resources from the NASA High-End Computing Program. We thank  
313 Bruce Van Aartsen for contributing to the GMI simulations. The CESM project is  
314 supported by the National Science Foundation and the Office of Science (BER) of the US  
315 Department of Energy. The MOPITT project is supported by the NASA Earth Observing  
316 System (EOS) Program. The National Center for Atmospheric Research (NCAR) is  
317 sponsored by the National Science Foundation.

318

319

320 Angelbratt, J., Mellqvist, J., Simpson, D., Jonson, J., Blumenstock, T., Borsdorff, T.,  
321 Duchatelet, P., Forster, F., Hase, F., Mahieu, E., De Maziere, M., Notholt, J., Petersen,  
322 A., Raffalski, U., Servais, C., Sussmann, R., Warneke, T., and Vigouroux, C.: Carbon  
323 monoxide (CO) and ethane (C<sub>2</sub>H<sub>6</sub>) trends from ground-based solar FTIR measurements  
324 at six European stations, comparison and sensitivity analysis with the EMEP model,  
325 Atmospheric Chemistry and Physics, 11, 9253-9269, 10.5194/acp-11-9253-2011, 2011.  
326 Bey, I., Jacob, D., Logan, J., and Yantosca, R.: Asian chemical outflow to the Pacific in  
327 spring: Origins, pathways, and budgets, Journal of Geophysical Research-Atmospheres,  
328 106, 23097-23113, 10.1029/2001JD000806, 2001.  
329 CRUTZEN, P.: DISCUSSION OF CHEMISTRY OF SOME MINOR CONSTITUENTS  
330 IN STRATOSPHERE AND TROPOSPHERE, Pure and Applied Geophysics, 106, 1385-  
331 1399, 10.1007/BF00881092, 1973.  
332 Deeter, M., Emmons, L., Edwards, D., Gille, J., and Drummond, J.: Vertical resolution  
333 and information content of CO profiles retrieved by MOPITT, Geophysical Research  
334 Letters, 31, 10.1029/2004GL020235, 2004.  
335 Deeter, M. N., Martinez-Alonso, S., Edwards, D. P., Emmons, L. K., Gille, J. C.,  
336 Worden, H. M., Pittman, J. V., Daube, B. C., and Wofsy, S. C.: Validation of MOPITT  
337 Version 5 thermal-infrared, near-infrared, and multispectral carbon monoxide profile  
338 retrievals for 2000-2011, Journal of Geophysical Research-Atmospheres, 118, 6710-  
339 6725, 10.1002/jgrd.50272, 2013.  
340 Duncan, B. N., Strahan, S. E., Yoshida, Y., Steenrod, S. D., and Livesey, N.: Model study  
341 of the cross-tropopause transport of biomass burning pollution, Atmospheric Chemistry  
342 and Physics, 7, 3713-3736, 2007.



- 343 Duncan, B. N., and Logan, J. A.: Model analysis of the factors regulating the trends and  
344 variability of carbon monoxide between 1988 and 1997, *Atmospheric Chemistry and*  
345 *Physics*, 8, 7389-7403, 2008.
- 346 Edwards, D. P., Emmons, L. K., Hauglustaine, D. A., Chu, D. A., Gille, J. C., Kaufman,  
347 Y. J., Petron, G., Yurganov, L. N., Giglio, L., Deeter, M. N., Yudin, V., Ziskin, D. C.,  
348 Warner, J., Lamarque, J. F., Francis, G. L., Ho, S. P., Mao, D., Chen, J., Grechko, E. I.,  
349 and Drummond, J. R.: Observations of carbon monoxide and aerosols from the Terra  
350 satellite: Northern Hemisphere variability, *Journal of Geophysical Research-*  
351 *Atmospheres*, 109, 10.1029/2004jd004727, 2004.
- 352 EPA: Our Nation's Air - Status and Trends through 2010, edited by: EPA-454/R-12-001,  
353 Research Triangle Park, NC, 2011.
- 354 Eyring, V., Lamarque, J.-F., Hess, P., Arfeuille, F., Bowman, K., Chipperfield, M. P.,  
355 Duncan, B., Fiore, A., Gettelman, A., and Giorgetta, M. A.: Overview of IGAC/SPARC  
356 Chemistry-Climate Model Initiative (CCMI) community simulations in support of  
357 upcoming ozone and climate assessments, *Sparc Newsletter*, 40, 48-66, 2013.
- 358 Frith, S., Kramarova, N., Stolarski, R., McPeters, R., Bhartia, P., and Labow, G.: Recent  
359 changes in total column ozone based on the SBUV Version 8.6 Merged Ozone Data Set,  
360 *Journal of Geophysical Research: Atmospheres*, 119, 9735-9751, 2014.
- 361 Granier, C., Bessagnet, B., Bond, T., D'Angiola, A., van der Gon, H. D., Frost, G. J.,  
362 Heil, A., Kaiser, J. W., Kinne, S., Klimont, Z., Kloster, S., Lamarque, J. F., Liousse, C.,  
363 Masui, T., Meleux, F., Mieville, A., Ohara, T., Raut, J. C., Riahi, K., Schultz, M. G.,  
364 Smith, S. J., Thompson, A., van Aardenne, J., van der Werf, G. R., and van Vuuren, D.  
365 P.: Evolution of anthropogenic and biomass burning emissions of air pollutants at global  
366 and regional scales during the 1980-2010 period, *Climatic Change*, 109, 163-190,  
367 10.1007/s10584-011-0154-1, 2011.
- 368 Gratz, L., Jaffe, D., and Hee, J.: Causes of increasing ozone and decreasing carbon  
369 monoxide in springtime at the Mt. Bachelor Observatory from 2004 to 2013,  
370 *Atmospheric Environment*, 109, 323-330, 10.1016/j.atmosenv.2014.05.076, 2015.
- 371 Guenther, A., Jiang, X., Heald, C., Sakulyanontvittaya, T., Duhl, T., Emmons, L., and  
372 Wang, X.: The Model of Emissions of Gases and Aerosols from Nature version 2.1  
373 (MEGAN2. 1): an extended and updated framework for modeling biogenic emissions,  
374 2012.
- 375 He, H., Stehr, J., Hains, J., Krask, D., Doddridge, B., Vinnikov, K., Canty, T., Hosley, K.,  
376 Salawitch, R., and Worden, H.: Trends in emissions and concentrations of air pollutants  
377 in the lower troposphere in the Baltimore/Washington airshed from 1997 to 2011,  
378 *Atmospheric Chemistry and Physics*, 13, 7859-7874, 2013.
- 379 Kurokawa, J., Ohara, T., Morikawa, T., Hanayama, S., Janssens-Maenhout, G., Fukui, T.,  
380 Kawashima, K., and Akimoto, H.: Emissions of air pollutants and greenhouse gases over  
381 Asian regions during 2000-2008: Regional Emission inventory in ASia (REAS) version  
382 2, *Atmospheric Chemistry and Physics*, 13, 11019-11058, 10.5194/acp-13-11019-2013,  
383 2013.
- 384 Li, L., and Liu, Y.: Space-borne and ground observations of the characteristics of CO  
385 pollution in Beijing, 2000-2010, *Atmospheric Environment*, 45, 2367-2372,  
386 <http://dx.doi.org/10.1016/j.atmosenv.2011.02.026>, 2011.
- 387 Naik, V., Voulgarakis, A., Fiore, A. M., Horowitz, L. W., Lamarque, J. F., Lin, M.,  
388 Prather, M. J., Young, P. J., Bergmann, D., Cameron-Smith, P. J., Cionni, I., Collins, W.



- 389 J., Dalsoren, S. B., Doherty, R., Eyring, V., Faluvegi, G., Folberth, G. A., Josse, B., Lee,  
390 Y. H., MacKenzie, I. A., Nagashima, T., van Noije, T. P. C., Plummer, D. A., Righi, M.,  
391 Rumbold, S. T., Skeie, R., Shindell, D. T., Stevenson, D. S., Strode, S., Sudo, K., Szopa,  
392 S., and Zeng, G.: Preindustrial to present-day changes in tropospheric hydroxyl radical  
393 and methane lifetime from the Atmospheric Chemistry and Climate Model  
394 Intercomparison Project (ACCMIP), *Atmospheric Chemistry and Physics*, 13, 5277-  
395 5298, 10.5194/acp-13-5277-2013, 2013.
- 396 Ohara, T., Akimoto, H., Kurokawa, J., Horii, N., Yamaji, K., Yan, X., and Hayasaka, T.:  
397 An Asian emission inventory of anthropogenic emission sources for the period 1980-  
398 2020, *Atmospheric Chemistry and Physics*, 7, 4419-4444, 2007.
- 399 Oman, L. D., Ziemke, J. R., Douglass, A. R., Waugh, D. W., Lang, C., Rodriguez, J. M.,  
400 and Nielsen, J. E.: The response of tropical tropospheric ozone to ENSO, *Geophysical*  
401 *Research Letters*, 38, 10.1029/2011gl047865, 2011.
- 402 Reynolds, R., Rayner, N., Smith, T., Stokes, D., and Wang, W.: An improved in situ and  
403 satellite SST analysis for climate, *Journal of Climate*, 15, 1609-1625, 10.1175/1520-  
404 0442(2002)015<1609:AIISAS>2.0.CO;2, 2002.
- 405 Riahi, K., Grübler, A., and Nakicenovic, N.: Scenarios of long-term socio-economic and  
406 environmental development under climate stabilization, *Technological Forecasting and*  
407 *Social Change*, 74, 887-935, 2007.
- 408 Rienecker, M. M., Suarez, M. J., Gelaro, R., Todling, R., Bacmeister, J., Liu, E.,  
409 Bosilovich, M. G., Schubert, S. D., Takacs, L., Kim, G.-K., Bloom, S., Chen, J., Collins,  
410 D., Conaty, A., da Silva, A., Gu, W., Joiner, J., Koster, R. D., Lucchesi, R., Molod, A.,  
411 Owens, T., Pawson, S., Pegion, P., Redder, C. R., Reichle, R., Robertson, F. R., Ruddick,  
412 A. G., Sienkiewicz, M., and Woollen, J.: MERRA: NASA's Modern-Era Retrospective  
413 Analysis for Research and Applications, *Journal of Climate*, 24, 3624-3648,  
414 10.1175/JCLI-D-11-00015.1, 2011.
- 415 Stein, O., Schultz, M., Bouarar, I., Clark, H., Huijnen, V., Gaudel, A., George, M., and  
416 Clerbaux, C.: On the wintertime low bias of Northern Hemisphere carbon monoxide  
417 found in global model simulations, *Atmospheric Chemistry and Physics*, 14, 9295-9316,  
418 10.5194/acp-14-9295-2014, 2014.
- 419 Strahan, S. E., Duncan, B. N., and Hoor, P.: Observationally derived transport diagnostics  
420 for the lowermost stratosphere and their application to the GMI chemistry and transport  
421 model, *Atmospheric Chemistry and Physics*, 7, 2435-2445, 2007.
- 422 Strode, S., Duncan, B., Yegorova, E., Kouatchou, J., Ziemke, J., and Douglass, A.:  
423 Implications of carbon monoxide bias for methane lifetime and atmospheric composition  
424 in chemistry climate models, *Atmospheric Chemistry and Physics*, 15, 11789-11805,  
425 2015a.
- 426 Strode, S. A., Rodriguez, J. M., Logan, J. A., Cooper, O. R., Witte, J. C., Lamsal, L. N.,  
427 Damon, M., Van Aartsen, B., Steenrod, S. D., and Strahan, S. E.: Trends and variability  
428 in surface ozone over the United States, *Journal of Geophysical Research: Atmospheres*,  
429 120, 9020-9042, 2015b.
- 430 THOMPSON, A.: THE OXIDIZING CAPACITY OF THE EARTH'S ATMOSPHERE -  
431 PROBABLE PAST AND FUTURE CHANGES, *Science*, 256, 1157-1165,  
432 10.1126/science.256.5060.1157, 1992.
- 433 Tilmes, S., Lamarque, J. F., Emmons, L. K., Kinnison, D. E., Marsh, D., Garcia, R. R.,  
434 Smith, A. K., Neely, R. R., Conley, A., Vitt, F., Val Martin, M., Tanimoto, H., Simpson,



- 435 I., Blake, D. R., and Blake, N.: Representation of the Community Earth System Model  
436 (CESM1) CAM4-chem within the Chemistry-ClimateModel Initiative (CCMI), Geosci.  
437 Model Dev. Discuss., 2016, 1-50, 10.5194/gmd-2015-237, 2016.
- 438 Tohjima, Y., Kubo, M., Minejima, C., Mukai, H., Tanimoto, H., Ganshin, A.,  
439 Maksyutov, S., Katsumata, K., Machida, T., and Kita, K.: Temporal changes in the  
440 emissions of CH<sub>4</sub> and CO from China estimated from CH<sub>4</sub>/CO<sub>2</sub> and CO/CO<sub>2</sub>  
441 correlations observed at Hateruma Island, Atmospheric Chemistry and Physics, 14, 1663-  
442 1677, 10.5194/acp-14-1663-2014, 2014.
- 443 van der Werf, G. R., Randerson, J. T., Giglio, L., Collatz, G. J., Mu, M., Kasibhatla, P.  
444 S., Morton, D. C., DeFries, R. S., Jin, Y., and van Leeuwen, T. T.: Global fire emissions  
445 and the contribution of deforestation, savanna, forest, agricultural, and peat fires (1997-  
446 2009), Atmospheric Chemistry and Physics, 10, 11707-11735, 10.5194/acp-10-11707-  
447 2010, 2010.
- 448 van Donkelaar, A., Martin, R. V., Leaitch, W. R., Macdonald, A. M., Walker, T. W.,  
449 Streets, D. G., Zhang, Q., Dunlea, E. J., Jimenez, J. L., Dibb, J. E., Huey, L. G., Weber,  
450 R., and Andreae, M. O.: Analysis of aircraft and satellite measurements from the  
451 Intercontinental Chemical Transport Experiment (INTEX-B) to quantify long-range  
452 transport of East Asian sulfur to Canada, Atmospheric Chemistry and Physics, 8, 2999-  
453 3014, 2008.
- 454 Voulgarakis, A., Marlier, M., Faluvegi, G., Shindell, D., Tsigaridis, K., and Mangeon, S.:  
455 Interannual variability of tropospheric trace gases and aerosols: The role of biomass  
456 burning emissions, Journal of Geophysical Research-Atmospheres, 120, 7157-7173,  
457 10.1002/2014JD022926, 2015.
- 458 Wang, Y., Munger, J., Xu, S., McElroy, M., Hao, J., Nielsen, C., and Ma, H.: CO<sub>2</sub> and its  
459 correlation with CO at a rural site near Beijing: implications for combustion efficiency in  
460 China, Atmospheric Chemistry and Physics, 10, 8881-8897, 10.5194/acp-10-8881-2010,  
461 2010.
- 462 Warner, J., Carminati, F., Wei, Z., Lahoz, W., and Attie, J.: Tropospheric carbon  
463 monoxide variability from AIRS under clear and cloudy conditions, Atmospheric  
464 Chemistry and Physics, 13, 12469-12479, 10.5194/acp-13-12469-2013, 2013.
- 465 Worden, H. M., Cheng, Y., Pfister, G., Carmichael, G. R., Zhang, Q., Streets, D. G.,  
466 Deeter, M., Edwards, D. P., Gille, J. C., and Worden, J. R.: Satellite-based estimates of  
467 reduced CO and CO<sub>2</sub> emissions due to traffic restrictions during the 2008 Beijing  
468 Olympics, Geophysical Research Letters, 39, 2012.
- 469 Worden, H. M., Deeter, M. N., Frankenberg, C., George, M., Nichitiu, F., Worden, J.,  
470 Aben, I., Bowman, K. W., Clerbaux, C., Coheur, P. F., de Laat, A. T. J., Detweiler, R.,  
471 Drummond, J. R., Edwards, D. P., Gille, J. C., Hurtmans, D., Luo, M., Martinez-Alonso,  
472 S., Massie, S., Pfister, G., and Warner, J. X.: Decadal record of satellite carbon monoxide  
473 observations, Atmospheric Chemistry and Physics, 13, 837-850, 10.5194/acp-13-837-  
474 2013, 2013.
- 475 Yin, Y., Chevallier, F., Ciais, P., Broquet, G., Fortems-Cheiney, A., Pison, I., and  
476 Saunois, M.: Decadal trends in global CO emissions as seen by MOPITT, Atmos. Chem.  
477 Phys., 15, 13433-13451, 10.5194/acp-15-13433-2015, 2015.
- 478 Yoon, J., Pozzer, A., Hoor, P., Chang, D., Beirle, S., Wagner, T., Schloegl, S., Lelieveld,  
479 J., and Worden, H.: Technical Note: Temporal change in averaging kernels as a source of



480 uncertainty in trend estimates of carbon monoxide retrieved from MOPITT, Atmospheric  
481 Chemistry and Physics, 13, 11307-11316, 10.5194/acp-13-11307-2013, 2013.  
482 Yoon, J., and Pozzer, A.: Model-simulated trend of surface carbon monoxide for the  
483 2001-2010 decade, Atmospheric Chemistry and Physics, 14, 10465-10482, 10.5194/acp-  
484 14-10465-2014, 2014.  
485 Yumimoto, K., Uno, I., and Itahashi, S.: Long-term inverse modeling of Chinese CO  
486 emission from satellite observations, Environmental Pollution, 195, 308-318,  
487 10.1016/j.envpol.2014.07.026, 2014.  
488 Zhang, Q., Streets, D. G., Carmichael, G. R., He, K. B., Huo, H., Kannari, A., Klimont,  
489 Z., Park, I. S., Reddy, S., Fu, J. S., Chen, D., Duan, L., Lei, Y., Wang, L. T., and Yao, Z.  
490 L.: Asian emissions in 2006 for the NASA INTEX-B mission, Atmospheric Chemistry  
491 and Physics, 9, 5131-5153, 2009.  
492 Zhao, Y., Nielsen, C. P., McElroy, M. B., Zhang, L., and Zhang, J.: CO emissions in  
493 China: Uncertainties and implications of improved energy efficiency and emission  
494 control, Atmospheric Environment, 49, 103-113, 10.1016/j.atmosenv.2011.12.015, 2012.  
495  
496



**Table 1:** Description of Simulations

Simulation	Model	Meteorology	Anthropogenic Emissions	Biomass Burning Emissions
G-Ref-C1	GEOSCC M	internally derived	MACCITY	MACCITY , GFED3 (2009-2010)
C-Ref-C1	CAM4- Chem	internally derived	MACCITY	MACCITY, then repeat 2008
Ref-C1- SD	GMI	MERRA	MACCITY	Same as GEOSCCM
EmFix	GMI	MERRA	Fixed at 2000	Fixed at 2000
AltEmis	GMI	MERRA	Strode et al [2015]	GFED3





**Table 2: Regional Trends and Correlations**

**a. Trends<sup>1,2</sup>**

	Years	E. USA	Europe	E. China	N. Hemisphere
G-Ref-C1 <sup>3</sup>	2000-2010	-2.2 (0.38)	-1.8 (0.42)	2.2 (1.1)	-0.76 (3.0)
C-Ref-C1 <sup>3</sup>	2000-2010	-3.4 (0.54)	-2.9 (0.50)	1.4 (1.4)	-0.90 (3.0)
Ref-C1-SD <sup>3</sup>	2000-2010	-2.4 (0.53)	-1.6 (0.59)	1.4 (1.1)	-0.76 (3.0)
EmFix <sup>3</sup>	2000-2010	1.3 (0.55)	1.5 (0.44)	2.1 (0.87)	0.96 (2.5)
AltEmis <sup>3</sup>	2000-2010	0.71 (0.73)	0.74 (0.66)	3.8 (1.4)	1.1 (3.4)
<i>MOPITT</i>	<i>2000-2010</i>	<i>-2.5 (0.64)</i>	<i>-1.8 (0.69)</i>	<i>-2.9 (1.8)</i>	<i>-1.4 (2.8)</i>
G-Ref-C1 <sup>3</sup>	2000-2011	-2.4 (0.33)	-1.9 (0.36)	1.9 (0.97)	-0.90 (2.5)
Ref-C1-SD <sup>3</sup>	2000-2011	-2.1 (0.43)	-1.7 (0.51)	1.3 (1.0)	-0.89 (2.6)
EmFix <sup>3</sup>	2000-2011	1.3 (0.43)	1.3 (0.39)	2.0 (0.79)	0.91 (2.1)
AltEmis <sup>3</sup>	2000-2011	0.56 (0.59)	0.50 (0.58)	3.3 (1.3)	0.89 (2.9)
<i>MOPITT</i>	<i>2000-2011</i>	<i>-2.5 (0.55)</i>	<i>-1.9 (0.59)</i>	<i>-2.9 (1.5)</i>	<i>-1.5 (2.4)</i>
<i>MOPITT</i>	<i>2000-2014</i>	<i>-2.1 (0.41)</i>	<i>-1.7 (0.43)</i>	<i>-3.1 (1.1)</i>	<i>-1.4 (1.7)</i>

<sup>1</sup>10<sup>16</sup> molec cm<sup>-2</sup> yr<sup>-1</sup>

<sup>2</sup>1-sigma uncertainty given in parentheses

<sup>3</sup>Simulation results convolved with MOPITT averaging kernel and a priori

**b. Correlation (r) with monthly MOPITT anomalies<sup>1</sup>**

	Years	E. USA	Europe	E. China	N. Hemisphere
G-Ref-C1	2000-2010	0.26	0.39	0.061	0.71
C-Ref-C1	2000-2010	0.23	0.36	0.18	0.62
Ref-C1-SD	2000-2010	0.43	0.51	0.39	0.73
EmFix	2000-2010	0.10	0.21	0.071	0.059
AltEmis	2000-2010	0.55	0.59	0.48	0.69
G-Ref-C1	2000-2011	0.25	0.37	0.046	0.72
Ref-C1-SD	2000-2011	0.41	0.51	0.36	0.73
EmFix	2000-2011	0.095	0.24	0.080	0.094
AltEmis	2000-2011	0.53	0.59	0.47	0.69

<sup>1</sup>Correlations are calculated from the de-trended and de-seasonalized time series.

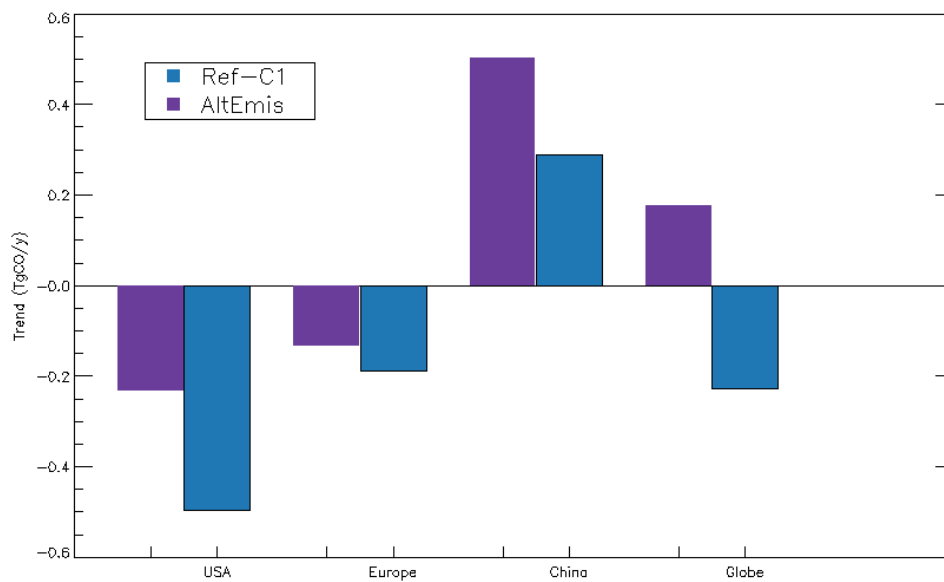


**Figure 1:** Trends in the CO emissions used in the Ref-C1 and Ref-C1-SD simulations (blue bars) and AltEmis simulation (purple bars) over 2000-2010 for the United States, Europe, China, and the world.

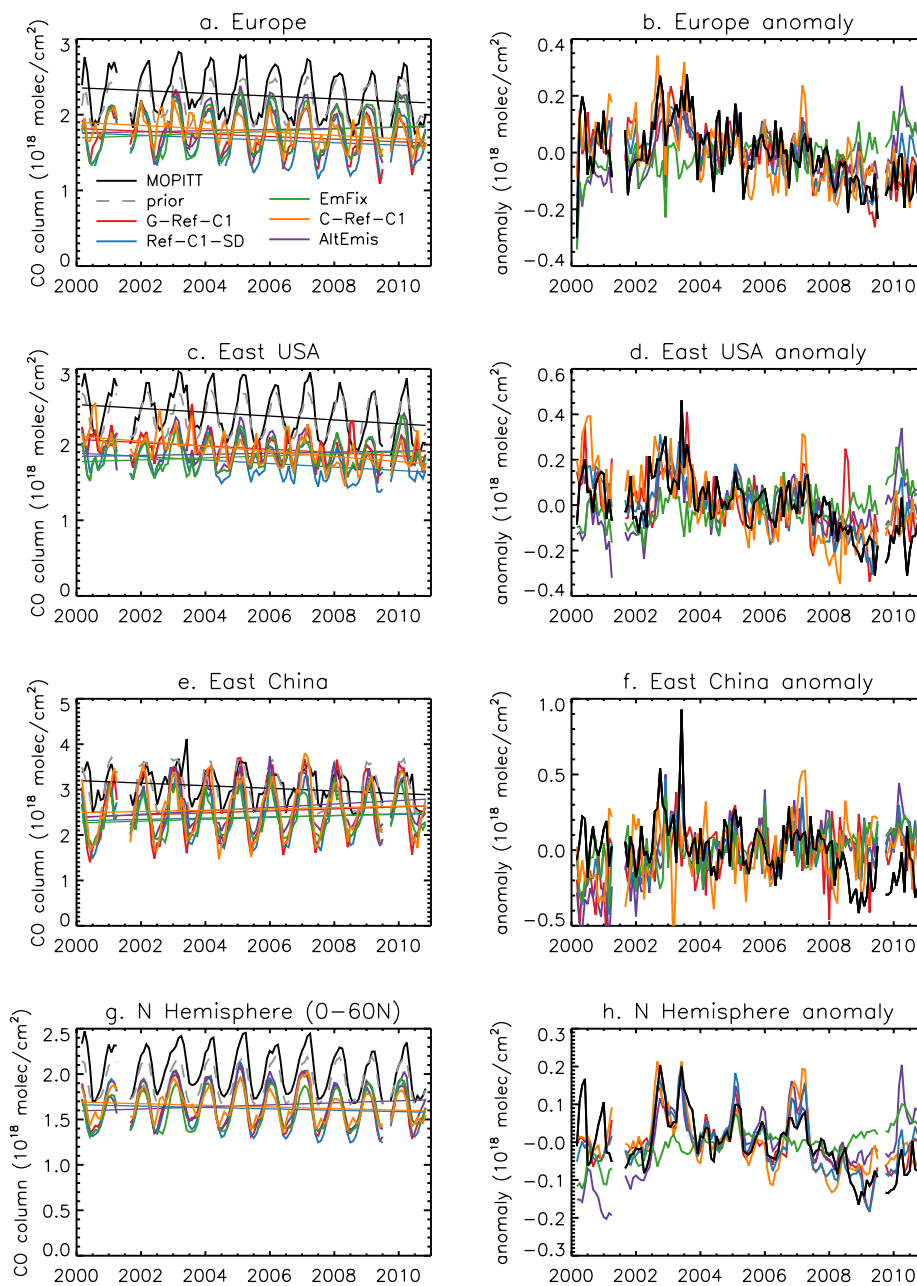


**Figure 2:** The time series and trends (left column) and de-seasonalized monthly anomalies (right column) of the CO column from MOPITT (black), the MOPITT a priori (gray), and simulated by G-Ref-C1 (red), Ref-C1-SD (blue), EmFix (green), C-Ref-C1 (orange), and AltEmis (purple) for 2000-2010.

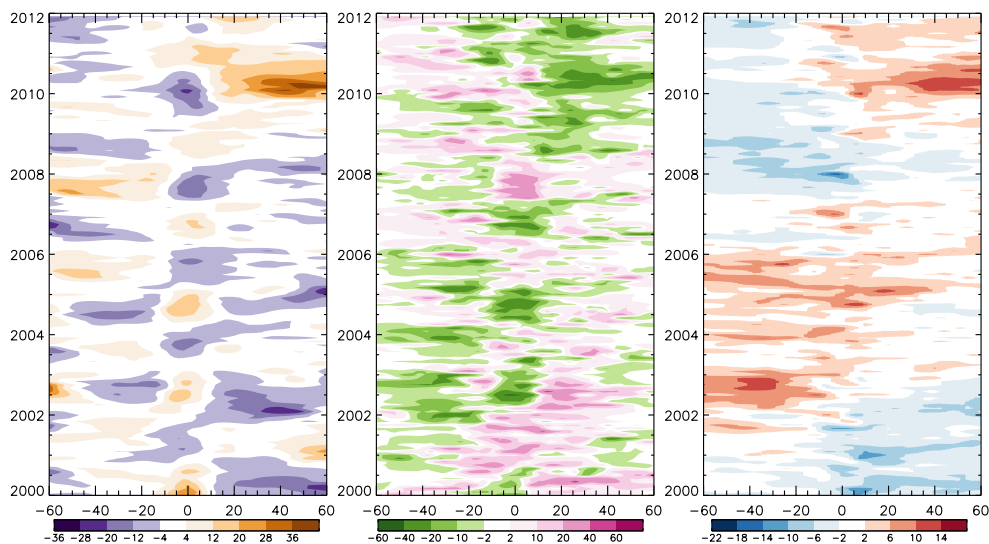


**Figure 3:** Deseasonalized monthly anomalies in the total ozone column (left), mean tropospheric OH (center), and CO column (right) from the EmFix simulation as a function of latitude and month.

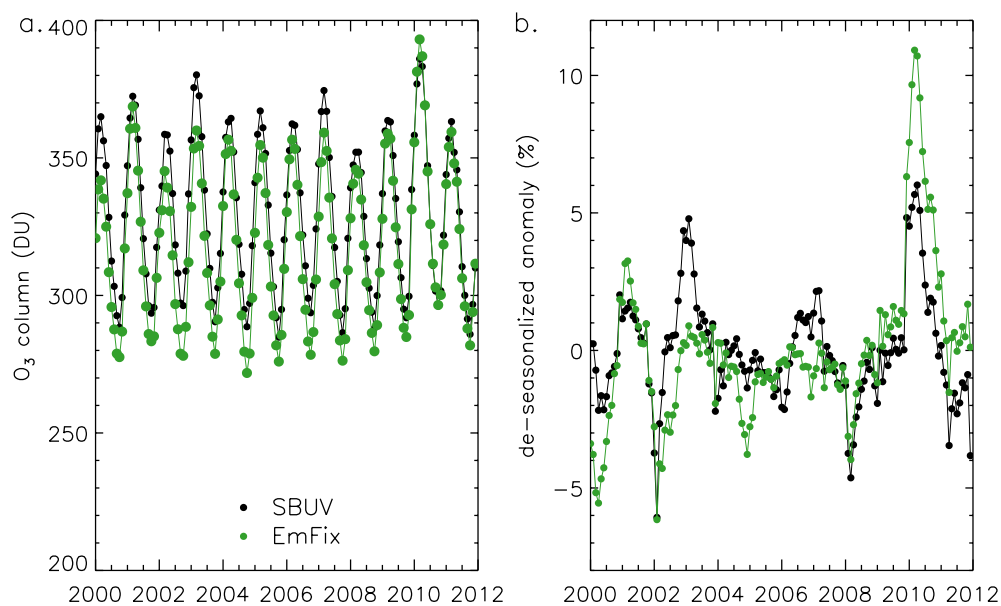


**Figure 4:** Monthly ozone column (a) and de-seasonalized ozone column anomaly (b) in SBUV data (black) and the EmFix simulation (green) for 30°-60°N.

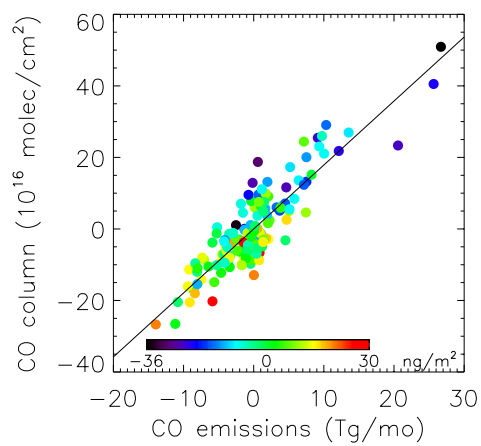


**Figure 5:** Monthly simulated CO column anomalies from the Ref-C1-SD simulation as a function of CO emissions for 10°S-10°N. Colors indicate the simulated OH column anomaly for the given month.